

MICROSCOPIC EVIDENCE FOR MICROBIAL DISSOLUTION OF SMECTITE

HAILIANG DONG^{1,*}, JOEL E. KOSTKA² AND JINWOOK KIM³

¹ Department of Geology, Miami University, Oxford, OH 45056, USA

² Oceanography Department, Florida State University, Tallahassee, FL 32306, USA

³ Naval Research Laboratory, CODE 7431, NASA Stennis Space Center, MS 39529, USA

Abstract—This study was undertaken to investigate mechanisms of mineral transformations associated with microbial reduction of structural Fe(III) in smectite. *Shewanella oneidensis* strain MR-1 cells were inoculated with lactate as the electron donor and Fe(III) in smectite as the electron acceptor. The extent of Fe(III) reduction was observed to reach up to 26%. Reduction proceeded via association of live bacterial cells with smectite. At the end of incubation, a large fraction of starting smectite was transformed to euhedral flakes of biogenic smectite with different morphology, structure, and composition. Lattice-fringe images obtained from environmental cell transmission electron microscope displayed a decrease of layer spacing from 1.5 ± 0.1 nm for the unreduced smectite to 1.1 ± 0.1 nm for the reduced smectite. The biogenic smectite contained more abundant interlayer cations, apparently as a result of charge compensation for the reduced oxidation state of Fe in the octahedral site. To capture the dynamics of smectite reduction, a separate experiment was designed. The experiment consisted of several systems, where various combinations of carbon source (lactate) and different concentrations of AQDS, an electron shuttle, were used. Selected area electron diffraction patterns of smectite showed progressive change from single-crystal patterns for the control experiment (oxidized, unaltered smectite), to diffuse ring patterns for the no-carbon experiment (oxidized, but altered smectite), to well-ordered single crystal pattern for the experiment amended with 1 mM AQDS (well crystalline, biogenic smectite). Large crystals of vivianite and fine-grained silica of biogenic origin were also detected in the bioreduced sample. These data collectively demonstrate that microbial reduction of Fe(III) in smectite was achieved via dissolution of smectite and formation of biogenic minerals. The microbially mediated mineral dissolution-precipitation mechanism has important implications for mineral reactions in natural environments, where the reaction rates may be substantially enhanced by the presence of bacteria.

Key Words—EC-TEM, Microbial Fe(III) Reduction, Mineral Transformation, *Shewanella oneidensis*, Smectite.

INTRODUCTION

Recent studies have demonstrated that mineral transformations associated with microbial reduction are complex and depend upon medium composition and the presence or absence of organic and inorganic ligands. Metal-reducing bacteria have been shown to be capable of reducing Fe(III) in amorphous hydrous oxide (Fredrickson *et al.*, 1998), crystalline Fe oxides such as goethite (Roden and Zachara, 1996; Zachara *et al.*, 1998; Cooper *et al.*, 2000; Liu *et al.*, 2001) and magnetite (Kostka and Nealson, 1995; Dong *et al.*, 2000), and silicate clays (Kostka *et al.*, 1999a, 1999b; Dong *et al.*, 2003). The mechanisms by which bacteria reduce Fe(III) in solid phases have been studied in the past (Fredrickson *et al.*, 1998; Kostka *et al.*, 1999a; Lovley, 2000; Dong *et al.*, 2000), but are still not well understood. It has been suggested that direct contact between cell and oxide surfaces is necessary for microbial respiration and reduction (Munch and Ottow, 1983). Recent studies have demonstrated that dissimilatory Fe-reducing bacteria can use humic substances and anthraquinone-2,6-disulfonate (AQDS) as electron

acceptors for respiration (Lovley *et al.*, 1996; Fredrickson *et al.*, 1998; Lovley *et al.*, 1998). The reduced organic compounds can, in turn, reduce Fe(III) in oxides, functioning as electron shuttles between oxides and cells. Certain metal-reducing bacteria have been shown to be capable of producing their own electron shuttles (Newman and Kolter, 2000; Nevin and Lovley, 2002), obviating the need for external electron shuttles.

Although it has been implied in several past studies that Fe(III) reduction by bacteria may involve dissolution of solid phases and precipitation of newly-formed biogenic minerals (Kostka *et al.*, 1999a, 1999b; Dong *et al.*, 2003), no direct observation has been made to confirm this hypothesis, particularly at the microscopic level. The objective of this study was to observe directly mineral phase transitions during microbial reduction of Fe(III) in smectite. We have investigated the influence of AQDS on the extent of Fe(III) reduction in smectite, and utilized scanning and transmission electron microscopy (SEM and TEM) to observe mineral transformations. A unique feature of this study was the employment of environmental cell (EC) TEM to study clay mineral transformations. In this study, we provide evidence for microbial dissolution of reactant smectite, and formation of morphologically, structurally and compositionally

* E-mail address of corresponding author:

dongh@muohio.edu

DOI: 10.1346/CCMN.2003.0510504

different, biogenic smectite, as well as biogenic vivianite and fine-grained silica.

MATERIALS AND METHODS

Bacteria, clay and reduction experiments

Shewanella oneidensis strain MR-1 and the ferruginous smectite were prepared and inoculated according to a procedure defined previously (Kostka *et al.*, 1999a, 1999b). Briefly, a minimal culture medium was used to grow MR-1 cells aerobically (Kostka and Nealson, 1998). The 0.5 to 2 μm size-fraction of the ferruginous smectite from the Source Clays Repository of The Clay Minerals Society was prepared (Kostka *et al.*, 1999b). The structural Fe content of the smectite clay was determined to be 3.549 mmol Fe/g (with <0.1 mmol/g of this Fe present as Fe oxide impurities) (Lear and Stucki, 1989).

Two separate experiments were conducted with the same electron donor and acceptor but different concentrations of AQDS and initial cell density. In both experiments, lactate (20 mmol/L final concentration) was added as the electron donor, and microwave radiation-sterilized smectite was added as the sole electron acceptor (2 g/L final concentration) in a minimal culture medium (Kostka *et al.*, 1999a). Both experiments were run for 2 months. Cell cultures and smectite clays were dispensed into serum bottles with rubber stoppers. Controls included heat-killed cells in the same medium in place of live ones. The concentrations of AQDS and initial cell density differed in the two experiments. In the first one, 1 mM AQDS was added to the treatment serum bottles. This experiment was considered non-growth incubation because the cells were at stationary phase and initial cell density was high ($\sim 2 \times 10^8$ cells/mL). In the second experiment, three different concentrations of AQDS were added (0, 0.1 and 1 mM). This experiment was designed to examine the effects of AQDS on reduction of Fe(III) in smectite and on cell growth. This experiment was considered growth incubation because log phase cells were used and initial cell density was low (1×10^5 cells/mL). In one treatment of the growth experiment, no lactate was added. Culture tubes were incubated at 30°C in the dark. All manipulations of culture media and samples were carried out under anoxic conditions within a Coy anaerobic chamber (90% N₂, 10% H₂) (Coy Laboratory Products, Ann Arbor, Michigan).

Analyses

For the non-growth experiment, Fe(II) production was analyzed at the end of incubation. For the growth experiment, Fe(II) production was measured as a function of time. At select time points, the culture tubes were removed from the incubator and analyzed for Fe(II) concentrations. The extent of microbial reduction of Fe(III) in smectite was measured by production of

Fe(II) by 0.5 N HCl extraction using ferrozine assay under strictly anoxic condition (Lovley and Phillips, 1986). Dissolved Fe, Al, Si, Mg, Na, K and Ca concentrations at the end of the incubation of the growth experiment were measured by direct current plasma (DCP) emission spectrometry. Because K and Na were major constituents of the minimal medium, their concentrations were not meaningful, and therefore not reported. Cell numbers at the end of the growth experiment were determined by direct counting using acridine orange and epifluorescence microscopy as described previously (Hobbie *et al.*, 1977). Bacterial direct counting procedures were modified for solid-containing suspensions (Proctor and Souza, 2001).

The mineral solids at the end of the incubation of both experiments were studied with SEM and TEM. Samples were prepared inside an anaerobic glove bag. To prepare samples for SEM observations, cell-mineral gels (suspensions) were fixed in 2.5% glutaraldehyde in a 0.05 M Na cacodylate buffer solution of pH 7. One droplet of fixed cell-mineral gel was placed on the surface of a glass cover slip that was cleaned with 1 $\mu\text{g}/\text{mL}$ polylysine solution prior to use. The sample was allowed to settle down onto the cover slip for 20 min. The sample-coated cover slips were sequentially dehydrated using varying proportions of ethanol and distilled water, followed by critical point drying. The cover slips were mounted onto SEM stubs and Au coated for observations using an Hitachi SEM. The only time that the samples were exposed to air was during critical point drying and Au coating. The SEM was operated at the accelerating voltage of 15 kV. A short working distance (6–10 mm) and low beam current (30–40 μA) were used to achieve the best image resolution. A longer working distance (15–20 mm) and higher beam current (50–70 μA) were used for qualitative energy dispersive spectroscopy (EDS) analysis. The beam size was of the order of tens to hundreds of nm.

Mineral solids for conventional TEM observations were fixed in 2.5% glutaraldehyde for at least 1 day. Due to concerns of decanting fine particles during subsequent dehydration steps, fine mineral particles were initially gently settled to the bottom of an eppendorf tube with a combination of gravity settling and centrifugation (several rpm). The semi-consolidated material was then encapsulated in 4% agar (w/w), and solidified agar (with encapsulated particles) was cut into cubes of 2–3 mm in size. The cubes were then placed in glass vials filled with 0.05 M sodium cacodylate buffer (pH = 7). The cubes were rinsed with the buffer four times, followed by a secondary fixation with 1% (w/w) osmium tetroxide (OsO₄) in the buffer for 2–3 h. The effectiveness of this fixation was manifested by color change of the cubes from green-colorless to black as cell constituents gradually reacted with OsO₄. The OsO₄ fixed cubes were rinsed with distilled water four times, followed by overnight staining with 0.05% (w/w) uranyl

acetate. The cubes were rinsed with distilled water again four times, and followed by sequential dehydration and embedding into L.R. White resin. Ultrathin sections (50–100 nm) were made from polymerized specimen blocks with a diamond knife (Delaware Diamond knife, Wilmington, DE) using a Reichert Ultracut E ultramicrotome. The ultrathin sections were coated with Au for TEM observations. High-resolution lattice-fringe imaging and chemical analyses were performed with a Philips CM12 scanning transmission electron microscopy (STEM) fitted with a Kevex Quantum solid-state detector and computer system. The STEM was operated at 120 kV and a beam current of 20 μA . A camera length of 770 nm and a selected-area aperture 10 μm in diameter were used to obtain selected area electron diffraction (SAED) patterns. Quantitative analytical electron microscope (AEM) analyses were obtained in the scanning mode by using a beam diameter of 50 \AA and a scanning area of $300 \times 300 \text{\AA}$. Standards and other conditions were similar to those defined previously (Dong and Peacor, 1996). High-resolution TEM images were taken at $100,000\times$.

The conventional TEM procedures are inadequate for observations of expandable clay mineral structures, such as that of smectite, because water-bearing smectite tends to dehydrate in the high-vacuum environment of conventional TEM, causing d_{001} layer-spacing collapse. For example, despite efforts to maintain the original layer spacing of nontronite by impregnation with Nanoplast, Kim *et al.* (2003) observed collapse of 001 layers in the conventional TEM electron column, making d_{001} of microbially reduced nontronite indistinguishable from that of unreduced material. Water exchange with methanol and infiltration with L.R. White resin has also been used to prevent clay layers from collapsing (Stucki and Tessier, 1991). However, the authors observed homogeneous layer spacing for both chemically reduced and non-reduced smectite, illustrating the limitations of

conventional TEM. For this reason, EC-TEM was employed to study the layer spacing of both unreduced and reduced smectite. A JEOL JEM-3010 transmission electron microscope operating at 300 keV with a LaB_6 filament was used in this study, and this system has been described previously (Daulton *et al.*, 2002; Kim *et al.*, 2003). For EC-TEM observations, mineral solids were separated from aqueous solution by centrifugation, and the pellet was rinsed with H_2O followed by re-suspension. Several microliters were loaded on the lower EC window, and the EC holder was then sealed and inserted into the TEM column. A flow of N_2 gas ($2 \text{ Torr L min}^{-1}$) saturated with water vapor was maintained in the EC during operation at pressures between 10 and 100 Torr. All lattice-fringe images were obtained at $250,000\times$ magnification with a 20 μm objective aperture. Multiple fringe spacings ($\sim 100\text{--}200$) were measured to obtain an average layer spacing and standard deviation for both unreduced and reduced smectite.

RESULTS

Reduction of Fe(III) in smectite by bacteria

The extent of microbial reduction of Fe(III) in smectite reached up to 13%, 22%, 26% for 0 mM, 0.1 mM and 1 mM AQDS, respectively, by the end of 77 h, after which further reduction was not significant. The addition of AQDS significantly increased the extent and rate of smectite reduction (Figure 1a) and promoted cell growth (Figure 1b). No Fe(II) was produced in either the heat-killed control or no-carbon treatment. For the non-growth experiment, the extent of reduction of Fe(III) in smectite by 77 h was similar to that for the 1 mM AQDS treatment of the growth experiment.

Characterization of oxidized, unaltered smectite

The oxidized, unaltered smectite sample showed a bulky texture in SEM images with no particular

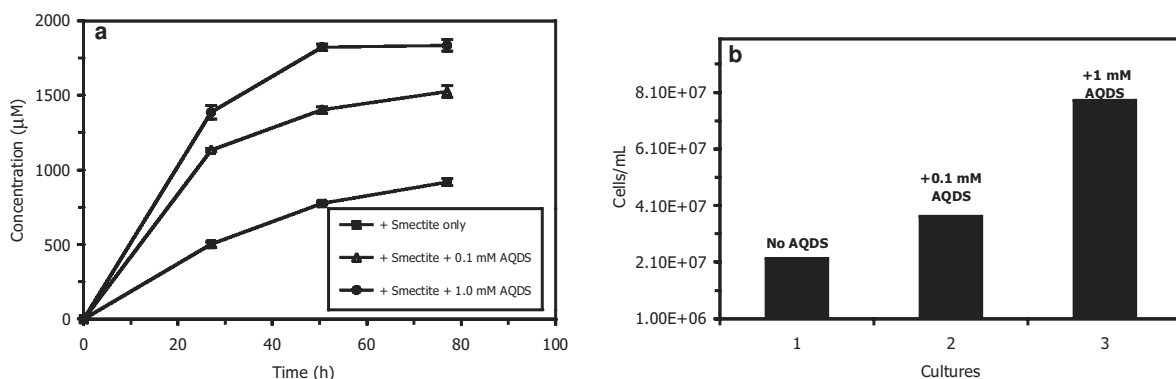


Figure 1. (a) 0.5 N HCl-extractable Fe(II) in smectite, smectite + 0.1 mM AQDS, and smectite + 1 mM AQDS of the growth experiment. The addition of AQDS enhanced the extent and the rate of microbial reduction of smectite. By the end of incubation, there was no production of Fe(II) in the heat-killed control and in the treatment with no carbon source. (b) Effect of AQDS on cell growth for the growth experiment. The incubation was run for two months for both experiments, but after 77 h, no significant Fe(II) was produced.

morphology (Figure 2a). Individual crystals could not be resolved. Lattice-fringe images obtained from conventional TEM showed varying spacing of smectite 001 layers, ranging from 1.1 to 1.4 nm, possibly reflecting a varying amount of dehydration in the electron column. A high-resolution EC-TEM lattice-fringe image showed 1.5 ± 0.1 nm layer spacing, with wavy and continuous layers and abundant layer terminations (Figure 2b). The $hk0$ SAED pattern showed diffuse rings suggesting small crystallites of smectite with random orientations with respect to one another. The qualitative SEM-EDS analyses showed typical composition of smectite with a relatively abundant Fe content (Figure 2c).

Electron microscopic data for mineral transformations

In the presence of 1 mM AQDS (non-growth experiment), the bioreduction proceeded via intimate association between bacterial cells and smectite as expected for enzymatic mediation of electron transfer to Fe(III) in

smectite (Figure 3). The individual bacteria were rod-shaped. At the end of the bioreduction experiment, euhedral flakes were produced (left-hand side of Figure 4). The qualitative SEM-EDS analyses revealed that those flakes were similar to smectite. The relatively well-defined crystal morphology of those flakes suggests that the crystals were different from the oxidized, unaltered smectite, and biogenic in origin (*i.e.* precipitated from solution).

Lattice-fringe images of bioreduced smectite (euhedral flakes) obtained from the conventional TEM displayed a range of layer spacing similar to that for the unreduced smectite, illustrating the problem of layer collapse in the electron column. The EC-TEM lattice-fringe image displayed relatively uniform fringe spacing of 1.1 ± 0.1 nm (Figure 5). These smectite layers occurred in packets with a mean packet thickness of ~ 5 – 10 layers. The contrast in the image was relatively uniform, indicating constant layer orientation of smectite

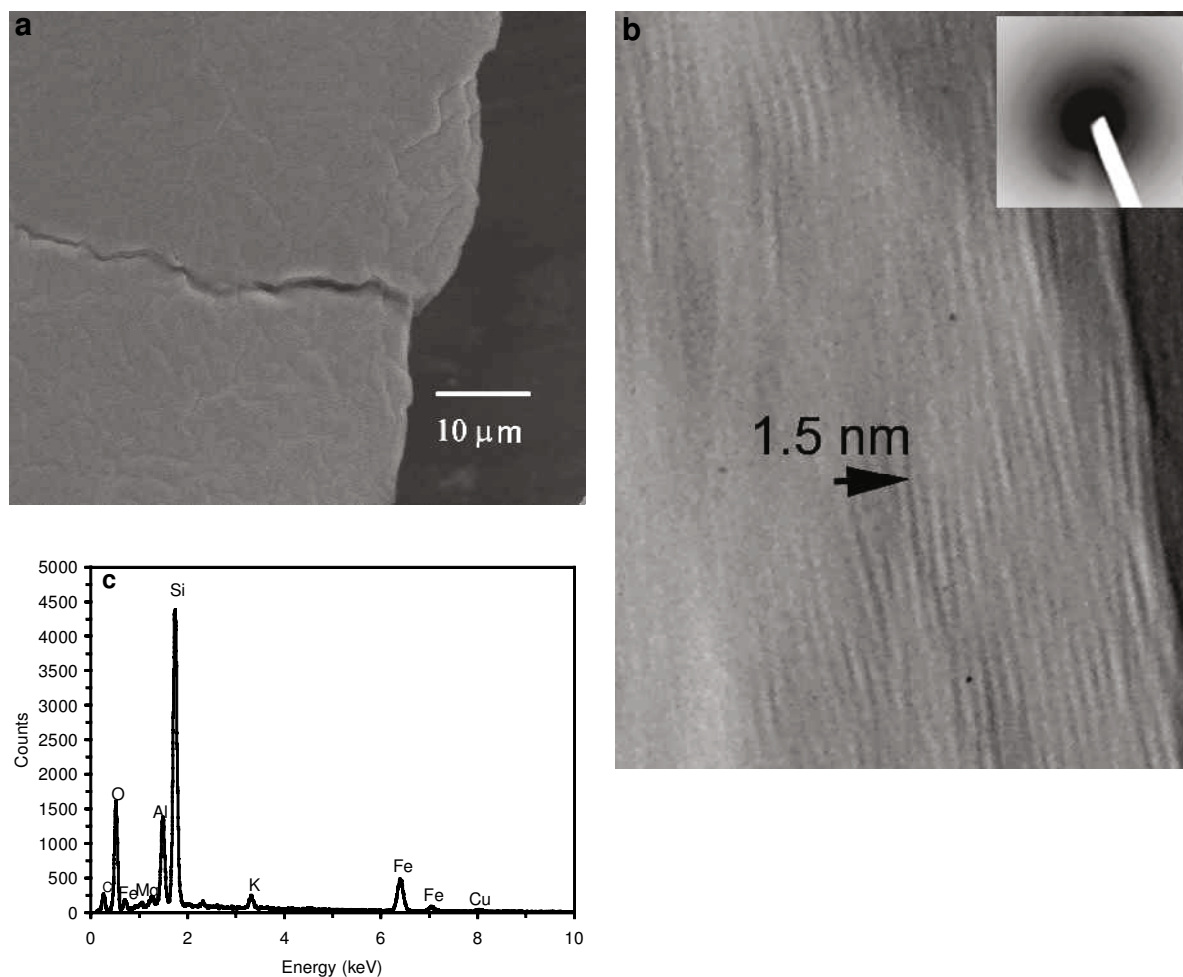


Figure 2. Secondary electron image (a), EC-TEM lattice-fringe image (b), and qualitative SEM-EDS spectrum (c) of the oxidized, unaltered smectite. The inset in part b is a $hk0$ SAED pattern showing diffuse rings. The 001 fringes are wavy and their orientations change by a few degrees over distances of several nanometers, resulting in difficulty in obtaining lattice-fringe images over a large area. Layer terminations are common.

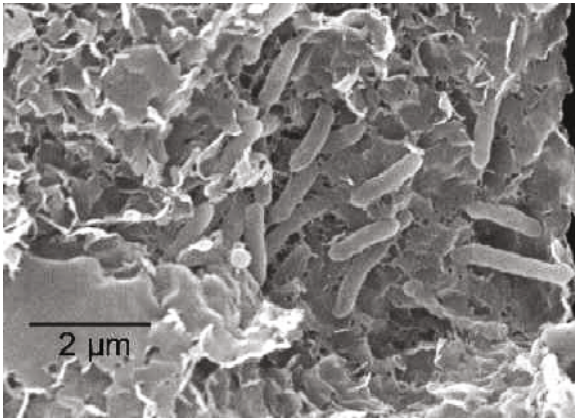


Figure 3. Secondary electron image showing bacteria in association with smectite.

layers with respect to the electron beam. Layer terminations were rare, and the corresponding SAED pattern showed well-defined reflections. These results are consistent with the observation by Gates *et al.* (1998) who noted an increased association between crystallite sub-units and an overall larger particle size. In addition to the presence of smectite in the solid phase at the end of the experiment, large crystals of vivianite (ferrous phosphate) were also detected (Figure 6a, large crystals on top and bottom of the image), as identified from the SEM-EDS composition (Figure 6b). In the control containing heat-killed cells, no mineral transformations were observed. The oxidized, unaltered smectite remained at the end of the incubations.

The effect of AQDS on mineral transformation was evident in the growth experiment. The oxidized, unaltered smectite in the heat-killed control showed a bulky, amorphous looking texture (Figure 7a) in SEM and spotty rings in its corresponding TEM SAED pattern (Figure 8a), suggesting that small crystallites of the oxidized, unaltered smectite were randomly oriented with respect to one another, but with some large, coherent ones giving rise to discrete reflections (Dong and Peacor, 1996; Freed and Peacor, 1992). In the treatment without a carbon source, the oxidized, unaltered smectite remained at the end of the incubation period (Figure 7b), but the rings in its SAED pattern became more diffuse (Figure 8b), and the discrete reflections no longer existed. This change in the SAED pattern suggests that, even in the absence of a carbon source, the oxidized, unaltered smectite was in part transformed to a randomly oriented, amorphous-like material, possibly getting ready for dissolution. In the presence of a carbon source but in the absence of AQDS, small euheedral crystals of smectite were observed (Figure 7c), suggesting the formation of new, biogenic smectite. The SAED pattern of those smectite crystals (Figure 8c) suggests that the newly formed, biogenic smectite crystals were largely randomly oriented with respect to one another. In the presence of 1 mM AQDS,

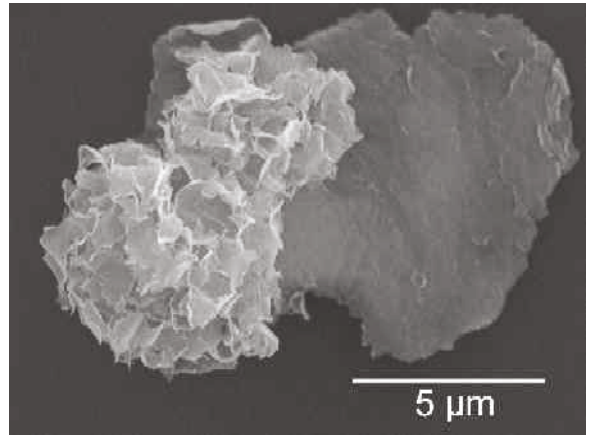


Figure 4. Secondary electron image showing mineral transformation from the oxidized, unaltered smectite (dark sheet on the right) to the biogenic smectite (euheedral crystals on the left).

euheedral smectite crystals were observed (Figure 7d). The SAED pattern showed a mixture of contributions from a dominant single crystal grain (hexagonal

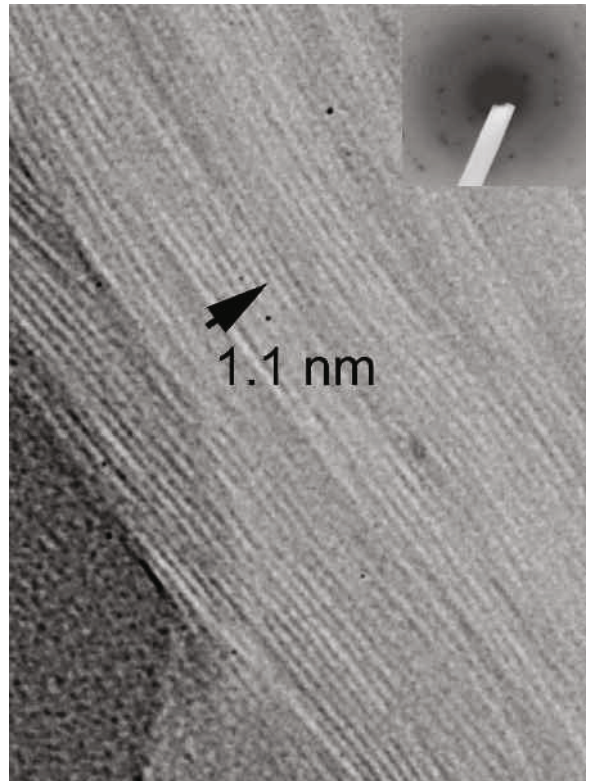


Figure 5. EC-TEM lattice-fringe image of biogenic smectite showing 1.1 nm layer spacing and its *hk0* SAED pattern. The smectite layers occur in packets with a packet thickness of 5–10 layers. The contrast is relatively uniform, and layer terminations are rare. The corresponding SAED pattern shows discrete reflections, reflecting some degree of coherence in smectite packets.

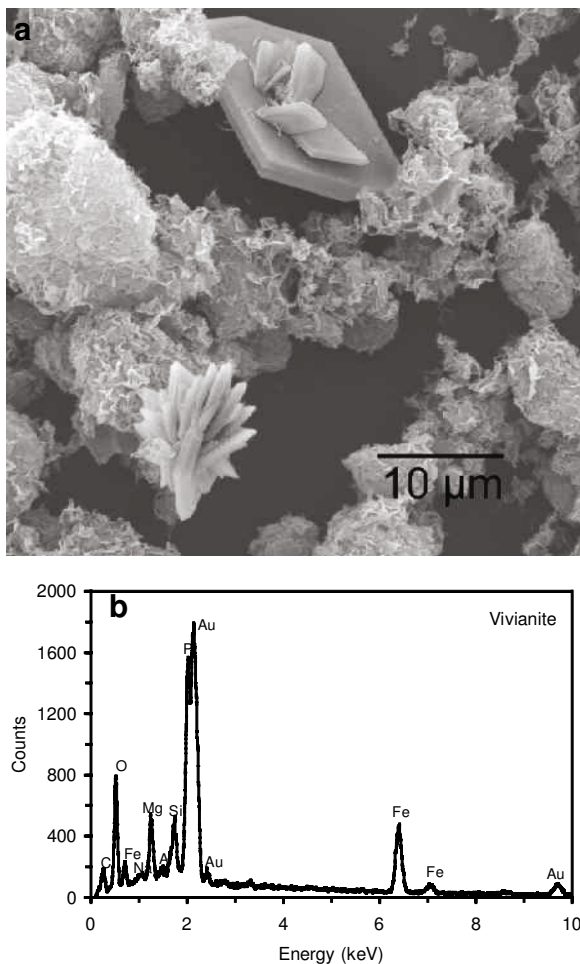


Figure 6. (a) Secondary electron image showing the presence of vivianite and euhedral smectite crystals in the bioreduced sample. (b) Qualitative SEM-EDS spectrum of vivianite showing typical vivianite composition. Some Si is derived from adjacent smectite.

symmetry) and smaller randomly oriented grains (concentric rings).

Changes in chemical composition accompanied the morphological and structural transformations of smectite as a result of bioreduction. Quantitative AEM analyses revealed that, relative to the composition of the oxidized, unaltered smectite, the biogenic smectite was more enriched in the interlayer cations, *i.e.* Ca, K and Na (Figure 9a). These excess cations were expected to balance the excess negative charge caused by the reduction of Fe(III) to Fe(II) in the octahedral site of the smectite structure. As expected for the ideal formula of smectite, the sum of octahedral Fe, Al and Mg in the oxidized, unaltered smectite was 4 per 12 tetrahedral and octahedral cations. However, this sum was significantly less than 4 in some biogenic smectite (Figure 9a). The octahedral (Fe+Al+Mg) content was inversely correlated with the Si content. In analyses of some biogenic smectite, the Si content was well in excess of 8, a

maximum value for the smectite formula based on 12 tetrahedral and octahedral cations. We term the Si excess as the difference between the AEM-measured Si content for the biogenic smectite (when normalized to 12 tetrahedral and octahedral cations) and that for the oxidized, unaltered smectite. The inverse correlation between the Si excess and the octahedral (Fe + Al + Mg) content in smectite (Figure 9b) indicated that each AEM analysis was actually obtained from two phases: a fine-grained, Si-rich phase and biogenic smectite. In those cases where the octahedral (Fe + Al + Mg) content approached the ideal value of 4, the Si excess was minimal, suggesting that inclusion of the Si-rich phase in the AEM analysis was minimal. When the octahedral (Fe + Al + Mg) content was well in deficit relative to the ideal value of 4, the Si excess was the largest, suggesting that the electron beam included a large proportion of the Si-rich phase. In some extreme cases, there was no inclusion of smectite, and pure Si was detected (Figure 10). No other elements were present in the quantitative TEM-EDS spectrum for the Si-rich phase, and the SAED pattern showed no reflections. Amorphous silica grains were of the order of several hundreds of nanometers in size. Based on these observations, we tentatively identified this phase as amorphous silica, biogenic in origin.

DCP data

Concentrations of Si, Fe, Mg and Ca in the treatments were substantially higher than those in the heat-killed control (Table 1), suggesting dissolution of oxidized, unaltered smectite, and release of its structural constituents to aqueous solution. The Al concentration for the treatments was not significantly different, and it was not stoichiometric to other ions in the solution, possibly due to precipitation of Al hydroxides at neutral pH. The Al solubility is lowest at neutral pH (Hem, 1985), and other studies have observed low Al concentration in aqueous solution in similar microbial reduction studies (Dong *et al.*, 2003). The aqueous concentrations of Si, Fe, Mg and Ca were similar at the three different concentrations of AQDS.

DISCUSSION

Superiority of EC-TEM in preserving original layer spacing of smectite

Despite our efforts to maintain the original layer spacing of smectite, we still observed the collapse of 001 layers of smectite in the conventional TEM electron column, making d_{001} of microbially reduced smectite hardly distinguishable from that of unreduced material. These observations are consistent with previous conventional TEM measurements of lattice-fringe spacings of smectites that show the same 001 layer spacing regardless of extent of reduction (Stucki and Tessier, 1991). Variable layer spacings of both unreduced and reduced

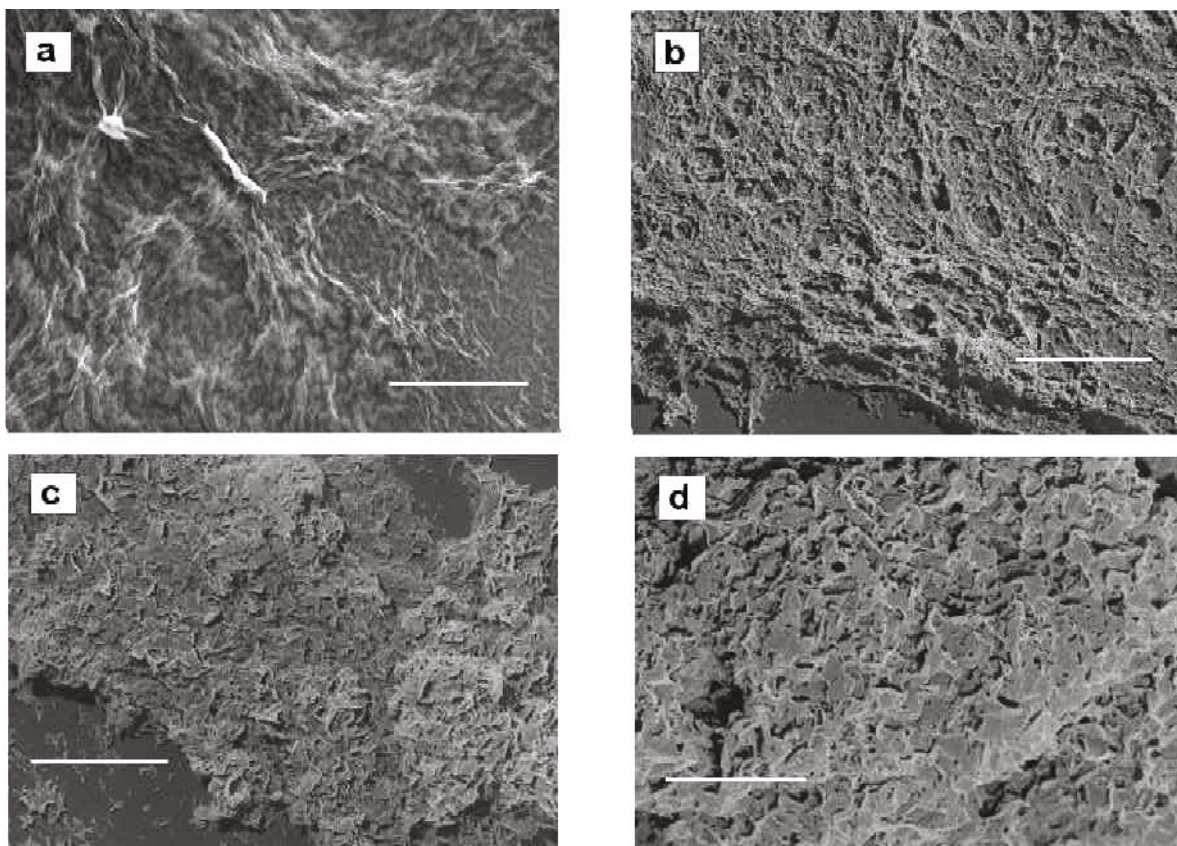


Figure 7. Secondary electron images of the oxidized, unaltered smectite in the heat-killed control (a), the oxidized, unaltered smectite in the treatment with no carbon source (b), biogenic smectite in the treatment with no AQDS (c), and biogenic smectite in the treatment with 1 mM AQDS. The scale bar on each image is 10 μm .

smectite in the present study suggest variable extent of preservation of the original layer spacing. In contrast, without any sample treatment, we observed reduction of d_{001} layer spacing from 1.5 ± 0.1 nm to 1.1 ± 0.1 nm as a result of microbial reduction of smectite. These results confirm the recent data by Kim *et al.* (2003) in their study on microbial reduction of nontronite, and demonstrate the great potential of this powerful technique to study microbe-clay interactions.

Mechanisms of microbial reduction of structural Fe

Although in the past decade significant evidence has accumulated that various bacteria are capable of reducing structural Fe(III) in minerals (Fredrickson *et al.*, 1998; Dong *et al.*, 2000; Fredrickson *et al.*, 2000; Lovley, 2000; Kukkadapu *et al.*, 2001; Liu *et al.*, 2001; Zachara *et al.*, 2001; Roden and Urrutia, 2002; Zachara *et al.*, 2002), the mechanisms of bioreduction have just begun to be understood (Newman and Kolter, 2000; Childers *et al.*, 2002; Nevin and Lovley, 2002). Most recent studies have suggested (Newman and Kolter, 2000) or demonstrated (Nevin and Lovley, 2002) that direct contact between Fe-reducing bacteria and Fe(III) minerals may not be necessary. In the presence of Fe³⁺

chelators or electron shuttles, Fe-reducing bacteria can reduce structural Fe(III) in crystalline minerals without direct contact. Under conditions where natural or synthetic electron shuttles are not present, Fe-reducing microorganisms of the genus *Shewanella* have been shown to produce their own electron-shuttling compounds, thereby aiding their Fe(III) reduction efficiency (Newman and Kolter, 2000; Nevin and Lovley, 2002). In this study, we have shown that upon extensive reduction of structural Fe(III) in smectite, biogenic smectite formed, even in the absence of AQDS. The AQDS enhanced the extent of bioreduction and crystallinity of biogenic smectite. *Shewanella oneidensis* strain MR-1 may also be capable of releasing extracellular quinones that could have served as an electron shuttle between cells and Fe(III) in the smectite structure. In the treatment with no carbon source, biogenic minerals were not observed. This is probably because cells were not metabolically active, and/or did not produce a significant amount of extracellular quinones.

This study contributes to the understanding of Fe(III) reduction mechanisms by showing that during the bioreduction process, reactant smectite was dissolved, and biogenic minerals formed. The formation of

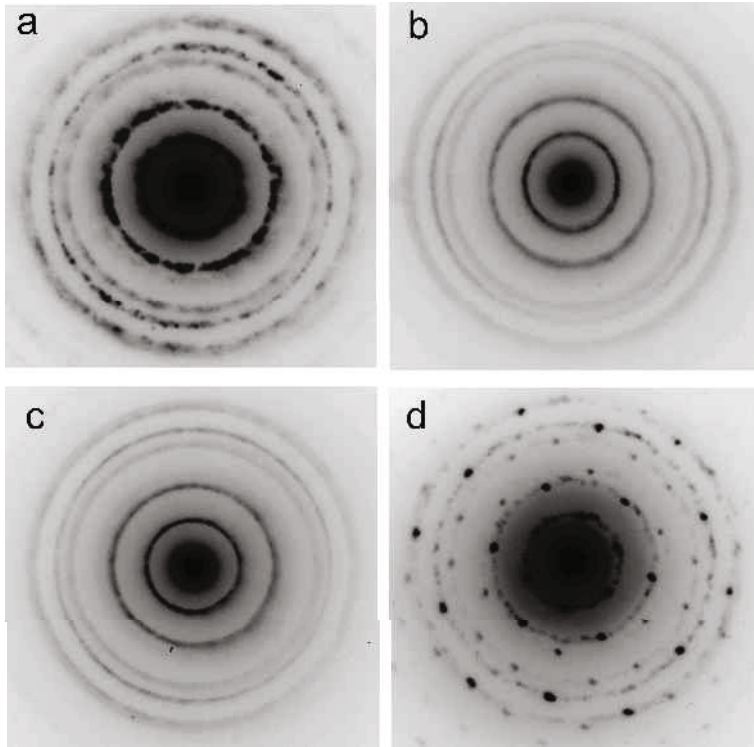
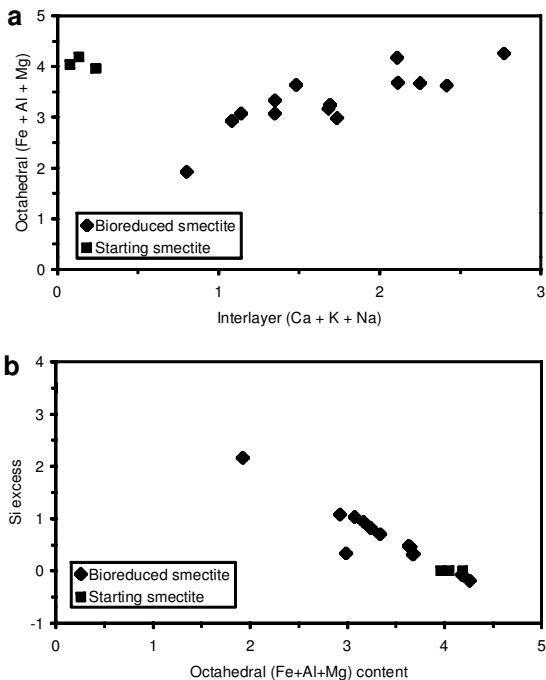


Figure 8. $hk0$ SAED patterns of the oxidized, unaltered smectite in the heat-killed control (a), in the treatment with no carbon source (b), biogenic smectite in the treatment with no AQDS (c), and in the treatment with 1 mM AQDS (d). The electron beam was normal to $\{001\}$ (or parallel to c^*).



biogenic smectite with distinct morphology, structure and composition suggests that the reactant smectite must have dissolved, and the bioproducted Fe(II) partitioned into biogenic smectite and vivianite structures. Furrer *et al.* (1993) determined the dissolution rates of Wyoming Na-montmorillonite to be $8.6 \times 10^{-13} \text{ mol m}^{-2} \text{ s}^{-1}$ to $4.3 \times 10^{-14} \text{ mol m}^{-2} \text{ s}^{-1}$ at pH of 1 to 5. Evaluations of the extent of smectite dissolution in our experimental time frame require determinations of crystal size of the oxidized, unaltered smectite. Three-dimensional crystal size of smectite is difficult to measure precisely, even by TEM. However, some approximation can be made. Assuming a smectite density of 2.6 g cm^{-3} , a parallelepiped shape, and the above-reported dissolution

Figure 9. (left) Quantitative AEM data for the oxidized, unaltered smectite and bioreduced smectite. The number of cations is normalized to 12 tetrahedral and octahedral cations (*i.e.* Si, Al, Fe and Mg). (a) Correlation between the octahedral cation (Fe + Al + Mg) and interlayer cations (Ca + K + Na); (b) Correlation between the Si excess and the octahedral cation (Fe + Al + Mg) for the starting and bioreduced smectite. The Si excess is defined as the difference between AEM-measured Si content for the bioreduced smectite (when normalized to 12 tetrahedral and octahedral cations) and that for the oxidized, unaltered smectite. The oxidized, unaltered smectite has 7.9 Si per 12 octahedral and tetrahedral cations, and by definition, it has a Si excess of 0.

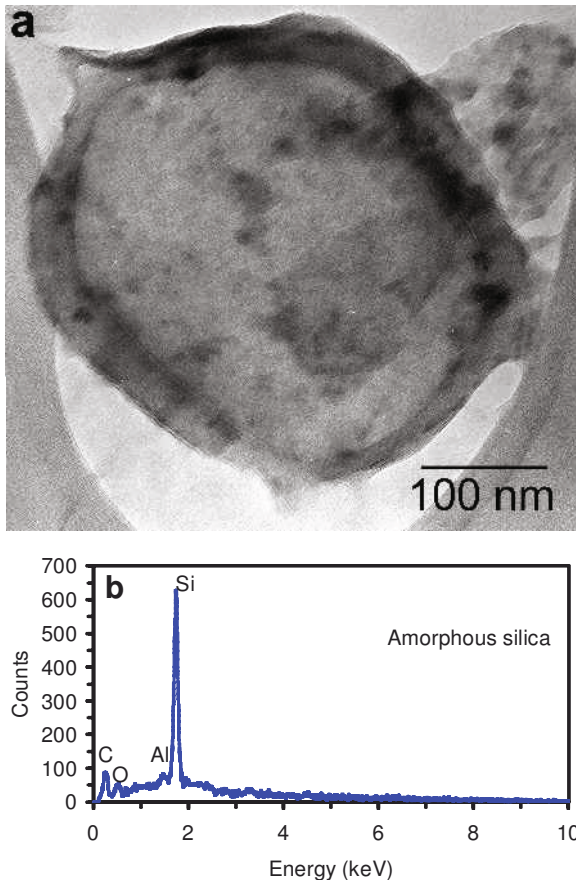


Figure 10. (a) TEM image of amorphous silica; (b) TEM-EDS spectrum of amorphous silica. The presence of a single Si peak is diagnostic of this phase.

rates, the minimum time is 3–30 days to dissolve a smectite crystal of $2 \times 2 \times 2 \mu\text{m}$ in size. An acidic pH could have existed at the smectite-cell interfaces, and this estimated dissolution time is certainly within our experimental time frame. The detection of biogenic vivianite and amorphous silica provides further evidence for the dissolution-precipitation mechanism. This mechanism has been shown to be important for microbial reduction of Fe oxides (Dong *et al.*, 2000; Fredrickson *et al.*, 2000), but this study has demonstrated its importance for clays.

What remains unclear is the relative order of Fe(III) reduction and smectite dissolution. Two scenarios are

possible. First, reduction of Fe(III) occurred in the solid state, causing a charge imbalance of the smectite structure. This charge imbalance may have triggered smectite dissolution and formation of biogenic minerals. Alternatively, bacterial cells may have produced organic acids and extracellular quinines, causing instability in the smectite structure, triggering smectite dissolution, and releasing structural Fe(III) to solution for microbial reduction. Soluble Fe^{3+} is present in natural environments, and has been suggested to be associated with humic substances (Luther *et al.*, 1996; Nevin and Lovley, 2002). The presence of soluble Fe^{3+} associated with electron shuttles in natural environments suggests that electron shuttles, such as humic substances, may be able to dissolve Fe(III) solids under favorable conditions. Direct contact between cells and smectite may also create microenvironments where pH and Eh conditions favor smectite dissolution.

The microbially mediated mineral dissolution-precipitation mechanism would have important implications for mineral reactions in natural environments where reaction rates may be substantially enhanced by the presence of bacteria, and natural waters may be geochemically altered by microbial processes. The microbially influenced mineral transformation mechanism makes it possible to form new, biogenic minerals, such as biogenic silica. The high aqueous silica concentration in the treatments, relative to the control, suggests that indeed, silica oversaturation may be possible under favorable conditions.

CONCLUSIONS

Smectite is very common in natural soils, sediments and sedimentary rocks. Because of its large surface area and high cation exchange capacity, it can affect the fate of pesticides, heavy metals and soil nutrients. In this study, we have presented multiple lines of evidence demonstrating that naturally present microbes can cycle smectite (dissolution of original smectite and formation of biogenic smectite, vivianite, and silica), thus altering the physical and chemical properties of smectite. Because both smectite and Fe-reducing bacteria are abundant in natural environments, the microbially mediated mineral transformations have important implications for many environmental processes, such as

Table 1. Aqueous concentrations of various ions.

	Heat-killed control (mg/g)	No carbon (mg/g)	0 mM AQDS (mg/g)	0.1 mM AQDS (mg/g)	1 mM AQDS (mg/g)
Mg	3.8	3.5±0.1	9.8±0.3	10.0±0.5	9.9±0.1
Si	3.7	5.0±0.9	30.4±0.5	29.8±0.6	30.3±0.7
Fe	1.3	1.6±0.3	3.0±0.2	3.4±0.1	3.6±0.4
Al	0.5	0.6±0.1	0.3±0.1	0.4±0.1	0.4±0.1
Ca	3.1	2.9±0.3	10.0±0.1	10.0±0.1	9.7±0.3

The elemental concentrations are expressed in mg/g of smectite

mineral weathering, nutrient cycling and contaminant transport.

ACKNOWLEDGMENTS

The authors are grateful to Drs John Morton and Richard Edelmann for their help in preparing the samples for DCP and electron microscopic analyses, respectively. Acknowledgment is made to the donors of The Petroleum Research Fund, administered by the American Chemical Society, for support (or partial support) of this research to HD (Grant # 36701-AC2). We are grateful to Joseph Stucki for the smectite sample. We are grateful to T. Daulton and one anonymous reviewer for their comments. JWK publishes with NRL contribution number 7430-03-2.

REFERENCES

- Childers, S.E., Ciuffo, S. and Lovley, D.R. (2002) Geobacter metallireducens accesses insoluble Fe(III) oxide by chemotaxis. *Nature*, **416**, 767–769.
- Cooper, D.C., Picardal, F., Rivera, J. and Talbot, C. (2000) Zinc immobilization and magnetite formation via ferric oxide reduction by *Shewanella putrefaciens* 200. *Environmental Science and Technology*, **34**, 100–106.
- Daulton, T.L., Little, B.J., Lowe, K. and Jones-Meehan, J. (2002) Electron energy loss spectroscopy techniques for the study of microbial chromium(VI) reduction. *Journal of Microbiological Methods*, **50**, 39–54.
- Dong, H. and Peacor, D.R. (1996) TEM observations of coherent stacking relations in smectite, I/S and illite of shales: evidence for MacEwan crystallites and dominance of 2M₁ polytypism. *Clays and Clay Minerals*, **44**, 257–275.
- Dong, H., Fredrickson, J.K., Kennedy, D.W., Zachara, J.M., Kukkadapu, R.K. and Onstott, T.C. (2000) Mineral transformation associated with the microbial reduction of magnetite. *Chemical Geology*, **169**, 299–318.
- Dong, H., Kukkadapu, R.K., Fredrickson, J.K., Zachara, J.M., Kennedy, D.W. and Kostandarites, H.M. (2003) Microbial reduction of structural Fe(III) in illite and goethite by a groundwater bacterium. *Environmental Science and Technology*, **37**, 1268–1276.
- Fredrickson, J.K., Zachara, J.M., Kennedy, D.W., Dong, H., Onstott, T.C., Hinman, N.W. and Li, S.M. (1998) Biogenic iron mineralization accompanying the dissimilatory reduction of hydrous ferric oxide by a groundwater bacterium. *Geochimica et Cosmochimica Acta*, **62**, 3239–3257.
- Fredrickson, J.K., Kostandarites, H.M., Li, S.W., Plymale, A.E. and Daly, M.J. (2000) Reduction of Fe(III), Cr(VI), U(VI), and Tc(VII) by *Deinococcus radiodurans* R1. *Applied and Environmental Microbiology*, **66**, 2006–2011.
- Freed, R.L. and Peacor, D.R. (1992) Diagenesis and the formation of authigenic illite-rich I/S crystals in Gulf Coast shales: TEM study of clay separates. *Journal of Sedimentary Petrology*, **62**, 220–234.
- Furrer, G., Zysset, M. and Schindler, P.W. (1993) Weathering kinetics of montmorillonite: investigations in batch and mixed-flow reactors. Pp. 243–262 in: *Geochemistry of Clay-Pore Fluid Interactions* (D.A.C. Manning, P.L. Hall and C.R. Hughes, editors). Mineralogical Society Series, **4**, Chapman & Hall, London.
- Gates, W.P., Jaunet, A.M., Tessier, D., Cole, M.A., Wilkinson, H.T. and Stucki, J.W. (1998) Swelling and texture of iron-bearing smectites reduced by bacteria. *Clays and Clay Minerals*, **46**, 487–497.
- Hem, J.D. (1985) *Study and interpretation of the chemical characteristics of natural water*. United States Government Printing Office, Washington, DC.
- Hobbie, J.E., Daley, R.J. and Jasper, S. (1977) Use of Nucleopore filters for counting bacteria by fluorescence microscopy. *Applied and Environmental Microbiology*, **33**, 1225–1228.
- Kim, J.W., Furukawa, Y., Daulton, T., Lavoie, D. and Newell, S. (2003) Characterization of microbially Fe(III)-reduced nontronite: environmental cell transmission electron microscopy. *Clays and Clay Minerals*, **51**, 382–389.
- Kostka, J.E. and Nealson, K.H. (1995) Dissolution and reduction of magnetite by bacteria. *Environmental Science and Technology*, **29**, 2535–2540.
- Kostka, J.E. and Nealson, K.H. (1998) Isolation, cultivation, and characterization of iron- and manganese-reducing bacteria. Pp. 58–78 in: *Techniques in Microbial Ecology* (R.S. Burlage, editor). Oxford University Press, Oxford, UK.
- Kostka, J.E., Haefele, E., Viehweger, R. and Stucki, J.W. (1999a) Respiration and dissolution of iron(III)-containing clay minerals by bacteria. *Environmental Science and Technology*, **33**, 3127–3133.
- Kostka, J.E., Wu, J., Nealson, K.H. and Stucki, J.W. (1999b) The impact of structural Fe(III) reduction by bacteria on the surface chemistry of smectite clay minerals. *Geochimica et Cosmochimica Acta*, **63**, 3705–3713.
- Kukkadapu, R.K., Zachara, J.M., Smith, S.C., Fredrickson, J.K. and Liu, C.X. (2001) Dissimilatory bacterial reduction of Al-substituted goethite in subsurface sediments. *Geochimica et Cosmochimica Acta*, **65**, 2913–2924.
- Lear, P.R. and Stucki, J.W. (1989) Effects of iron oxidation state on the specific surface area of nontronite. *Clays and Clay Minerals*, **37**, 547–552.
- Liu, C., Kota, S., Zachara, J.M., Fredrickson, J.K. and Brinkman, C.K. (2001) Kinetic analysis of the bacterial reduction of goethite. *Environmental Science and Technology*, **35**, 2482–2490.
- Lovley, D.R. (2000) *Environmental Microbe-Metal Interactions*. ASM press, Washington, D.C., 408 pp.
- Lovley, D.R. and Phillips, E.J.P. (1986) Availability of ferric iron for microbial reduction in bottom sediments of the fresh water tidal Potomac River. *Applied and Environmental Microbiology*, **52**, 751–757.
- Lovley, D.R., Coates, J.D., Blunt-Harris, E.L., Philips, E.J.P. and Woodward, J.C. (1996) Humic substances as electron acceptors for microbial respiration. *Nature*, **382**, 445–448.
- Lovley, D.R., Fraga, J.L., Blunt-Harris, E.L., Hayes, L.A., Philips, E.J.P. and Coates, J.D. (1998) Humic substances as a mediator for microbially catalyzed metal reduction. *Acta Hydrochimica et Hydrobiologica*, **26**, 152–157.
- Luther, G., Shellanbarger, P. and Brendel, P. (1996) Dissolved organic Fe(III) and Fe(II) complexes in salt marsh porewaters. *Geochimica et Cosmochimica Acta*, **60**, 951–960.
- Munch, J.C. and Ottow, J.C.G. (1983) Reductive transformation mechanism of ferric oxides in hydromorphic soils. *Environmental Biogeochemistry and Ecology Bulletin*, **35**, 383–394.
- Nevin, K.P. and Lovley, D.R. (2002) Mechanisms for Fe(III) oxide reduction in sedimentary environments. *Geomicrobiological Journal*, **19**, 141–159.
- Newman, D.K. and Kolter, R. (2000) A role for excreted quinones in extracellular electron transfer. *Nature*, **405**, 93–97.
- Proctor, L.M. and Souza, A. (2001) Method for enumeration of 5-cyano-2,3-ditylotetrazolium chloride (CTC)-active cells and cell-specific activity of benthic bacteria in riverine, estuarine, and coastal sediments. *Journal of Microbiological Methods*, **43**, 213–222.
- Roden, E.E. and Urrutia, M.M. (2002) Influence of biogenic Fe(II) on bacterial crystalline Fe(III) oxide reduction. *Geomicrobiological Journal*, **19**, 209–251.
- Roden, E.E. and Zachara, J.M. (1996) Microbial reduction of

- crystalline Fe(III) oxides: influence of oxide surface area and potential for cell growth. *Environmental Science and Technology*, **30**, 1618–1628.
- Stucki, J.W. and Tessier, D. (1991) Effects of iron oxidation state on the texture and structural order of Na-nontronite gels. *Clays and Clay Minerals*, **39**, 137–143.
- Zachara, J.M., Fredrickson, J.K., Li, S.-M., Kennedy, D.W., Smith, S.C. and Gassman, P.L. (1998) Bacterial reduction of crystalline Fe³⁺ oxides in single phase suspensions and subsurface materials. *American Mineralogist*, **83**, 1426–1443.
- Zachara, J.M., Fredrickson, J.K., Smith, S.C. and Gassman, P.L. (2001) Solubilization of Fe(III) oxide-bound trace metals by a dissimilatory Fe(III) reducing bacterium. *Geochimica et Cosmochimica Acta*, **65**, 75–93.
- Zachara, J.M., Kukkadapu, R.K., Fredrickson, J.K., Gorby, Y.A. and Smith, S.C. (2002) Biomineralization of poorly crystalline Fe(III) oxides by dissimilatory metal reducing bacteria (DMRB). *Geomicrobiological Journal*, **19**, 179–207.

(Received 17 September 2002; revised 12 May 2003; Ms. 718; A.E. Peter J. Heaney)